Explaining doping in material research (Hf substitution in ZnO films) by directly quantifying the van der Waals force

Chia-Yun Lai[1¥], Sergio Santos[1¥*], Toni Moser[1,2], Boulos Alfakes[3], Jin-You Lu[1,3],Tuza Olukan[1,3], Nitul Rajput[3*], Tobias Boström[1], Matteo Chiesa[1,3*]

[1]Department of Physics and Technology, UiT The Artic University of Norway, 9037 Tromsø, Norway

[2]Institut für Ionenphysik und Angewandte Physik, University of Innsbruck, 6020 Innsbruck, Austria

[3]Laboratory for Energy and NanoScience (LENS), Khalifa University of Science and Technology, Masdar Institute Campus, Abu Dhabi, UAE

[¥] Equally contributing author

[*] Corresponding email:

S.S: ssantos78h@gmail.com

N.R: nitul.rajput@ku.ac.ae

M.C: matteo.chiesa@uit.no

Abstract

Non-monotonic behavior has been observed in the optoelectronic properties of ZnO thin films as doped with Hf (HZO). Here we propose that two competing mechanisms are responsible for such behaviour. Specifically, we propose that provided two crystal orientations dominate film growth, only one of them might be responsible for direct Hf substitution. Nonmonotonic behaviour is expected at once by considering that preferential growth of the crystal that allows for direct Hf substitution is inhibited by Hf concentration in the manufacturing process. This inhibition would also be a thermodynamic consequence of Hf substitution. Maxima in Hf substitution is thus reached at a point where enough crystals exhibit the preferential orientation and where enough Hf is present on the surface for substitution. Outside such optimum scenario, Hf substitution can only decrease. We interpret the surface phenomena by discussing surface energy and the van der Waals forces as measured experimentally by means of atomic force microscopy.

Keywords: ZnO, doping, Hafnium, vdW, AFM

I. Introduction

Solid-state physics has provided a unified theory to the semiconductor industry for almost a century and has greatly advanced mathematically partially due to the possibility of modelling the atomic arrangement in crystals[1]. Semiconductors deal with theoretically interesting physical phenomena, such as band structure, that greatly impact our everyday lives[2-5] while the field also forms part of a high-tech and capital-intensive industry[6]. For this reason, it is not only exotic or unique properties that scientists are after, but rather practical parameters such as material cost, availability of resources and material property enhancement also enter into the equation and into a market of great impact in economy further affecting the overall advance of technology. In this respect, material doping is a process that can affect materials in technology both in terms of cost and as a resource on one hand and in terms of property enhancement on the other. Doping has therefore attracted major attention since the beginning[7]. In particular, doping has been a key parameter enabling the fine-tuning of properties such as band gap, electron affinity and mobility and, more generally, electrical and optical properties[8] while turning materials that where otherwise not practically useful into key technological parts and devices.

Property orthogonality would be highly advantageous in many applications since it would allow independently manipulating single properties at a time without disrupting others. Controllably adjusting material properties is important enough that it is partly driving both material development and characterization standards at the research level[9]. Besides the interest in crystal band structures, it has arguably been surface phenomena and bonding mechanisms at the very surface of semiconductors, particularly in silicon, that has led to major breakthroughs in the field[10, 11]. Research dealing with the process of doping semiconductor nanocrystals has also shed light

into the importance of surface phenomena with surface morphology and crystal shape directly affecting experimental outcomes against doping predictions[7]. In this respect, we recently[8] presented a very detailed characterization of Hf-doped ZnO films demonstrating high tunability of both electrical and optical properties with potential applications to photovoltaics and photonic devices in general. While Hf doping of Zn films is promising for several reasons, several key factors in the fabrication of the films are to be determined. In particular, it is found that band gap, resistivity, carrier concentration and work function first increase at the low Hf concentration (doping) regime and then peak to then decrease. This is in contrast with theoretical predictions showing that these properties should[8], in principle, monotonically increase with Hf as Hf atoms substitute the Zn atoms in the matrix.

The motivation of this paper deals with the non-monotonic behavior of the optoelectronic properties of ZnO thin films doped with Hf (HZO). In this article, we claim that the empirically observed non-monotonic behaviour suggests the presence of two competing surface mechanisms and we propose to discuss them in terms of van der Waals (vdW) surface forces. The two competing mechanism scenario that we put forward allows us to describe how the monotonic increase of one term, i.e. crystal plane growth in the 002 orientation with increasing Hf doping concentration, competes with the other, i.e. substitution of Hf mostly in the domains -100 planes - of the HZ0 films where the appearance of crystal planes monotonically and necessarily decreases with increasing 002 presence. We provide some evidence corroborating this hypothesis in the form of 1) theoretical DFT data predicting a monotonic increase of surface energy with Hf substitution into the Zn matrix, 2) high-resolution TEM (HRTEM) images and data reporting the monotonic increase of 002 crystal planes against the 100 orientation with increasing Hf concentration, 3)

atomic force microscopy data (AFM) transformed into surface energy and 4) van der Waals maps and an interpretation that is shown to be coherent with our hypothesis.

II. Methods

A. Fabrication and characterization

ZnO and HZO were deposited on a Si substrate using atomic layer deposition (ALD). This method provides uniform composition and controllable film thickness at a relatively low temperature that conforms to substrate surfaces as described elsewhere[8, 12]. HZO films were deposited on Si (100) substrates using an Oxford FlexAL ALD system and diethyl-zinc (DEZ), tetrakisethylmethylaminohafnium (TEMAH) and H_2O vapor as precursors. Growth temperature and pressure were set to 250°C and 200 mTorr. Si substrates were cleaned with acetone, isopropanol and DI water and then dried in N_2. Before each deposition, a dummy wafer was subjected to 90 cycles of a plasma HfO_2 recipe purging the line of the TEMAH precursor.

A dual beam FIB system (Thermo Fisher Scientific, Helios 650) was used to prepare the lamellae for TEM imaging with Pt capping layer and precursor gas $(CH_3)_3Pt(CpCH_3)$) as per the method described elsewhere[13]. For the TEM study, an image corrected TEM system (Thermo Fisher Scientific, Titan G2) with an X-field emission gun (X-FEG) source was operating at 300 kV. The Cypher AFM from Asylum Research was operated in amplitude modulation AM AFM mode. Standard OLYMPUS cantilevers AC160TS ($k\approx30$ N/m, $Q\approx300$, $f_{(1)0}\approx300$ kHz) and AC240TS ($k\approx2$ N/m, $Q\approx100$, $f_{(1)0}\approx$ 70kHz) were used throughout. For standard imaging, a scanning rate of 1Hz and an oscillation amplitude of ~7nm were employed. For reconstructing tip-sample interaction force, amplitude A and phase Φ versus tip-sample separation distance d curves were

recorded and the Sader-Jarvis-Katan formalism was exploited to transform the cantilever dynamics into the force versus distance curves. Full details of this procedure can be found elsewhere[14]. For bimodal imaging, the first 2 resonance frequencies of AC240TS cantilevers were used[15]. The tip radius R was monitored throughout all the experiments with the critical amplitude (A_C) method in order to ensure that R remained constant[16]. DFT calculations were performed employing similar parameters and methods as in previous studies[8]. Nevertheless, we still provide the main parameters relevant to this study as follows: all DFT simulations were performed using the Quantum Espresso package[28]. The Perdew Burke Ernzerhof (PBE) functional in generalized gradient approximations (GGA) with ultra-soft pseudopotential was used for the exchange-correlation energy. The DFT-D2 method of Grimme was applied for the van der Waals corrections, and the kinetic energy cutoffs and density cutoffs were set to 80/600 Ry. The Brillouin zone was sampled with a grid of 4 × 4× 4 k-points within the Monkhorst−Pack scheme. Before the substitution of Hf ions, all atomic positions of the bulk ZnO system with 32 atoms were allowed to fully relax until the Hellmann−Feynman force on each ion and total energy changes, were < 0.001 Ry/au and 1 × 10−6 Ry, respectively. The cohesive energy of doped ZnO systems was calculated according to the equation: $E_{form} = (E_{tot} - aE_{Zn} - bE_O - cE_{Hf})/N$, where E_{form} is the cohesive energy of a solid and refers to the energy required to separate constituent atoms apart from each other so to bring them to an assembly of neutral free atoms. The term *E* is the total energy of the system. The *a*, *b*, and *c* parameters correspond to the number of individual constituent atoms. Finally N is the total number of atoms inside the unit cell.

In terms of our terminology and regarding concentrations, we consider ZnO undoped films and 3 cases of doping. The doped cases we consider correspond to low (L), medium (M) and high (H) doping as shown in Table I. These three cases (ZnO (HZO) doped films) were prepared as summarized in Table I. The doped ZnO films are labelled according to the different Zn:Hf cycles that were used in the manufacturing process, *i.e*. 9, 1 and 0.5, and during ALD deposition (HZO-L, HZO-M and HZO-H, respectively).

Table I. Different Hf dopant concentration regimes for the ZnO (HZO) films. Four cases are considered including the undoped case ZnO (undoped) and low (L), medium (M) and high doping (H).

	ZnO	HZO-L	HZO-M	HZO-H
Cycles (Zn:Hf)	N/A	9	1	0.5
at.%	0	0.1	0.4	0.3

B. AFM force models

Our target in the AFM experiments was to characterize the sample's surface as a function of Hf concentration and to explain the non-monotonic behavior of material properties as detailed in the introduction. We chose to inspect the force quantitatively operating the AFM in ambient conditions and quantifying the van der Waals contribution by considering variations in surface energy. We also assume that the phenomena describing the attractive part of the force between the tip and the sample are captured in terms of atomic/molecular density ρ and atomic bond polarizability C. First,

we invoke the relationships between adhesion force or F_{AD} and surface energy γ [17]. These are standard[17] when interpreting AFM force maps:

$$F_{AD} \equiv 4\pi R\gamma \quad (1)$$

$$F_{AD} \equiv \frac{RH}{6a_0^2} \quad (2)$$

where R is the effective AFM tip radius, H is the Hamaker constant as described in detail below and a_0 is an intermolecular distance to avoid matter interpenetration as required by the Pauli exclusion principle. The value of a_0 is typically taken to be approximately 0.2 nm[17, 18]. In the bimodal AM AFM mode of operation, we map H directly by assuming Eqs. (1) and (2) and by exploiting the 3 free observables, i.e. φ_1 for the phase of the first mode and A_2 and φ_2 for the amplitude and phase of the second mode, that are available in AM AFM. This can be shown to result in a close form solution for H as described elsewhere[19].

Eqs. (1) and (2) provide the relationship we seek between minima in tip-sample force F_{AD}, surface energy γ and (atomic) van der Waals (vdW), i.e. specifically reduced to account for London dispersion, interactions. The latter contribution can be considered by modelling the effect of the atomic/molecular densities ρ of the interacting atoms and invoking the Hamaker approach [20]. In this model, particle-particle force interaction pairs between the atoms of the tip and the atoms of the sample's surface sum up to account for the net attractive tip-sample force F_{ts}. The C coefficient results from the particle–particle pair interactions in vdW models assuming a power law of 7 (6 when considering potential energies instead) as also standardly recognized as valid. The Hamaker can thus be written in the form already provided by Hamaker as:

$$H \equiv \pi \rho_{tip} \rho_s C_{tip/s} \quad (3)$$

where s stands for sample. Assuming (1) to (3) , considering the ratios of the force of adhesion only and assuming that R is constant while scanning and while reconstructing the tip-sample force throughout the experiments, the mechanism for the sample's contrast can be identified by considering the following equation:

$$\frac{\gamma_{tip/HZO}}{\gamma_{tip/ZnO}} = \frac{\rho_{HZO} C_{tip/HZO}}{\rho_{ZnO} C_{tip/ZnO}} \quad (4)$$

In (4) we find the vdW contributions from the atomic densities of the sample's surface atoms/molecules ρ and C as discussed above already. In summary, Eq. (4) provides two parameters controlling the contrast obtained in AFM experiments when imaging in the attractive regime and in terms of vdW forces. Formally, and in order to quantify the interaction in this study, one is the atomic density, as captured by atomic densities ρ in gr/cm^3 of the surface of the sample and the other is the atomic phenomena dependent magnitude for the particle-particle interaction as captured by the parameter C. We note that in order to deal with the very last atoms of the surface, and considering that the vdW force is relatively short range, i.e. physically relevant for sharp tips R~10 nm only at fractions of nm in the direction normal to the sample's surface, we will interpret the phenomena via ρ only and considering the very top layer of atoms only. That is, in terms of atoms/m^2. This last assumption is meaningful in our study as we will discuss later. In this work we further deal with the two crystal orientations that are typically considered to dominate the crystal orientation space of ZnO and HZO films. These are the 100 and 002 orientations as shown in Fig. 1 by HRTEM.

III. Discussion

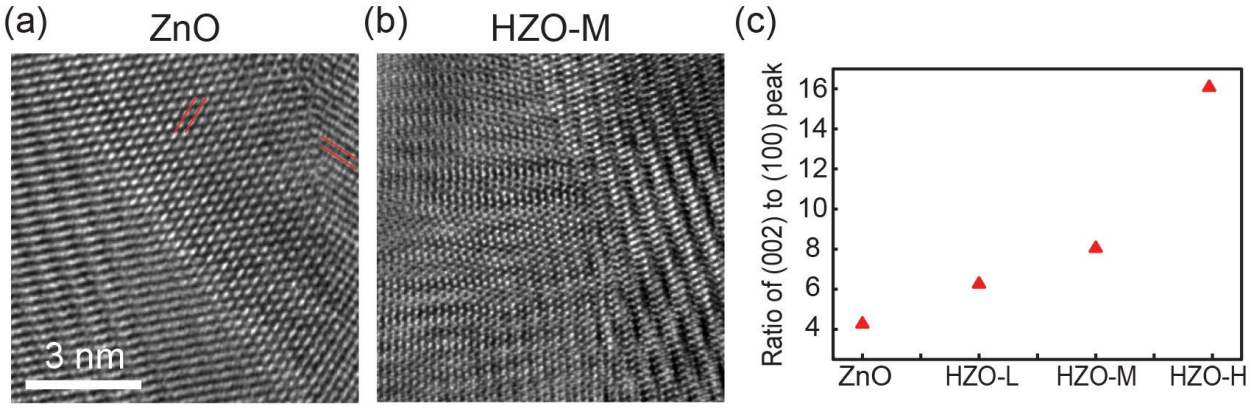

Figure 1. HRTEM images for undoped ZnO film (a), and HZO-M film (b). The shifting of crystal planes by integrating XRD peaks with increasing doping concentration (c).

The high-resolution TEM (HRTEM) image in Figure 1(a) confirms the polycrystallinity of the ZnO films. We also show an HRTEM image obtained for the HZO-M case (Figure 1(b)). The shift in preferential orientation in the ZnO crystal plane (from (100) to (002)) can be observed as a function of increasing Hf doping concentration (Figure 1(c)). This is the first result that we exploit in order to invoke monotonic versus non-monotonic behaviour. In particular, an analysis of crystal orientation as a function of Hf doping could only explain monotonic behaviour according to this result. We recall that our motivation here is to explain the non-monotonic behaviour of the optoelectronic parameters as described in the introduction and elsewhere[8, 21] in the literature. Such non-monotonic behaviour should occur by monotonically increasing Hf concentration in the fabrication process. While it does not follow from what we have found so far that Hf is in fact being substituted into the ZnO matrix, something which would mean that we have

arrived to the conclusion in our study, it does follow that explaining non-monotonic behaviour by the monotonic increase illustrated in Figure 1 alone would be problematic at best. Our second relevant result is illustrated in Figure 2. In short, according to our DFT calculations, substitution of Hf into the matrix also results in monotonic increase in surface energy (Figure 2). Surface energy as "explained" in AFM however relates to work of adhesion because it is, in principle, a two-body problem, i.e. tip and sample. The parameter known as "surface energy" of substitution systems cannot be computed via DFT directly either, not only because of not constituting a two-body problem – unless the two bodies are modelled and this is not the case here – but because of the DFT computational method in itself. Nearest-neighbor broken bond models[22] have shown however that the concept of "cohesive energy" is proportional to "surface energy"[23] thought of as energy that is free on account of interrupting bond formation on the surface, i.e. because of surface creation alone. In any case, for the sake of our question here, it is enough to observe that surface energy should in fact increase monotonically with Hf substitution according to DFT. The details of the DFT simulation have been already discussed in the methods section above under the title fabrication and characterization.

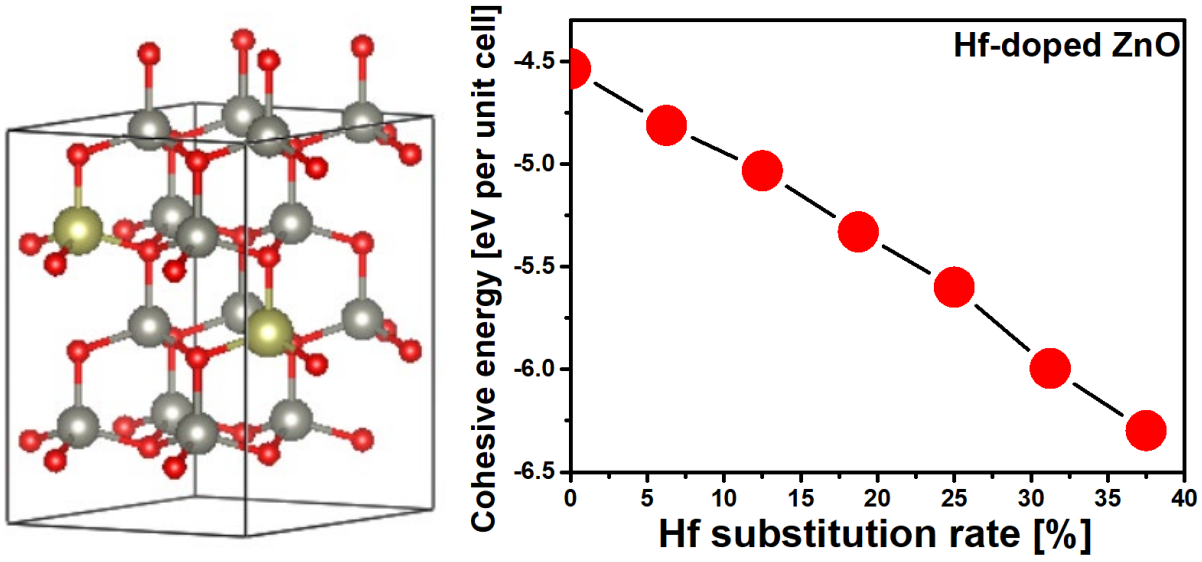

Figure 2. Illustration of the atomic structure used in the DFT simulations. The pattern shows that the effect on surface energy as a function of Hf substitution on a ZnO matrix is monotonic.

Atomically, we can employ the simple model in (1) to (4) to show why such monotonic behaviour as illustrated by Figures 1 and 2 could not explain the non-monotonic phenomena that we are dealing with here. We describe the magnitude of the C parameter qualitatively only and relate it to the polarizability of the bonds in the sample's crystal structures. But first let us qualitatively and semi-quantitatively consider the atomic number of the Hf atom versus that of the Zn atom. We see that their atomic mass ratio is approximately $178.49/65.38 \approx 2.7$. A consideration of atomic masses alone, and while noting that there are also oxygen atoms present in the matrix of the film and possibly exposed to the top atomic layer also[24], leads us to a contradiction in our interpretation when we combine it with the findings illustrated in Figures 1 and 2 and with the AFM data that we will discuss next. That is, if we consider surface atomic density alone and assume that there is

a direct increase in the substitution of atoms with increasing doping concentrations, we arrive to the conclusion that we should observe an increase in tip-sample surface energy with increasing Hf concentration. This would be a consequence of a density increases ρ in the numerator of (4) with increasing substitution. Since monotonic Hf substitution throughout could not result in the non-monotonic behavior of the optoelectronic properties observed experimentally, and as expected theoretically if that were the case, and again, as in the case of the phenomena of crystal orientation (Figure 1), we are not justified to simply invoke one to one correspondence. In summary, we cannot expect that Hf substitutes Zn monotonically with increasing Hf concentration in the process of fabrication. Nevertheless, we are now justified to expect, at least in terms of mean values, that surface energy will not increase monotonically with increasing Hf concentration throughout. In short, such experimental observation would contradict, to a first approximation, the relationship between direct Hf substitution and the surface energy increase expected in Figure 2 and in our simple atomic mass considerations for Eqs. (1) to (4). In fact, the situation would be worse if we also considered the implications of bond polarization via C. Again, to a first approximation and considering the Pauling's electronegativity parameter that describes the tendency of a given atom to attract a given electron in a bond, we find that the Hf to Oxygen bond results in electronegativity differences of 2.14 versus the 1.8 for the Zn to Oxygen bonds. We do not claim to have derived here in detail the exact relationship between the van der Waals force, electronegativity, the parameter C in Eq. (4) and the complex tip-sample interaction resulting from this, i.e. our model is too simple and the tip-sample interaction is known to be extremely complex in many cases. Nevertheless, as a first qualitative and semi-quantitative approximation, and with regard to monotonicity of behavior, or lack thereof, our considerations point to 1) the impossibility of claiming that there is a monotonic increase in Hf substitution into the Zn with increasing Hf

concentration in the manufacturing process and to the 2) expectation to observe non-monotonic behavior in mean surface-energy in the AFM data.

We are now at a point to state our claim clearly, namely, we propose that direct Hf substitution occurs mostly where the 100 crystal orientation is observed. Therefore, the overall mechanism for Hf-Zn direct substitution is a function of both 1) 100 to 200 crystal orientation presence or ratio (Figure 1) and 2) Hf concentration during sample preparation, or, as in our experiments, as a function of cycles as shown in Table I and as discussed in the methods section and elsewhere[8]. Our physical interpretation is that direct Hf substitution increases with Hf concentration mostly where the 100 crystal orientation is observed. If the 002 to 100 ratio remained constant during preparation, Hf substitution would monotonically increase at least until reaching some form of thermodynamic saturation. Nevertheless, since the presence of the 002 crystal orientation also increases in the matrix with increasing Hf concentration during the fabrication process (Figure 1), there is a point where increasing the concentration results in less 100 crystals and any excess Hf will simply not substitute. Non-monotonic behaviour follows at once if the above two statements are assumed.

In order to quantitatively interpret our claims, we invoke a simple model dealing with mean surface energy as measured with the AFM for a given surface area SA that is large enough to contain enough crystals, i.e. some with 002 orientation and some with 100 orientation. This allows us to employ statistics in our discussion. We recall that we are to account for the 1) non-monotonic behaviour of the optoelectronic properties of the HZO matrix (from previous studies and as discussed in the introduction), 2) the increase in the 002 versus 100 ratio of crystal orientation

(Figure 1) and 3) the requirement that Hf substitution into the matrix leads to larger surface energy (Figure 2 and explanation above via Eqs. (1) to (4)).

We start by considering presence of 100 crystal orientation M(100) versus presence of 002 crystal orientation N(002). Normalising these over an arbitrary surface area SA and assuming that only these two orientations constitute the whole we can write the identity:

$$M + N = 1 \quad (5)$$

It is expected that N will increase (M will decrease) with increasing Hf concentration, or cycles, during fabrication (Table I and Figure 1). Now we assume the mean surface energy across a given SA in the ZnO or HZO film to be $\underline{\gamma}$. We can now write the net contributions to $\underline{\gamma}$ from N and M, i.e. the ratio between 002 to 100 (Figure 1). Assuming that the mean surface energy $\underline{\gamma}(002)$ or $\underline{\gamma}_{002}$ associated with the 002 crystal orientation remains constant with increasing Hf concentration, i.e. Hf does not directly substitute for this orientation, the contribution to $\underline{\gamma}$ (for the areas SA under consideration) due to the 002 crystals can be written as $N\underline{\gamma}_{002}$. The normalised presence of the crystal 002 is given by N. This contribution is a function of N only since there is no change in $\underline{\gamma}_{002}$ as we assume there is no substitution for this orientation. Similarly, the contribution due to the 100 orientation is $M\underline{\gamma}_{100}$ for a mean surface energy of this crystal $\underline{\gamma}(100)$ or $\underline{\gamma}_{100}$ and a normalised presence of the crystal 100 given by M. We understand that M decreases monotonically (Figure 1) and we assume that $\underline{\gamma}_{100}$ increases monotonically due to Hf direct substitution (Figure 2 and discussion above). In particular we write $\underline{\gamma}_{100}$ =f(Hf concentration), a situation not assumed to be the case for the 002 crystals where $\underline{\gamma}_{002}$ is a constant. The combination of contributions can now

be expressed as a function of surface energies per crystal and the presence of N(002) only by using the identity in (5):

$$\underline{\gamma}=N(\underline{\gamma}_{002} - \underline{\gamma}_{100})+ \underline{\gamma}_{100} \quad (6)$$

or alternatively

$$\underline{\gamma}=\underline{\gamma}_{002}N + \underline{\gamma}_{100}(1-N)$$

Let us further assume that $\underline{\gamma}(002) > \underline{\gamma}(100)$ for the ZnO undoped films. This condition implies that, thermodynamically, it would be favourable for the film to contain a larger number of crystals in, and therefore that crystal growth would preferably occur following mainly, the 100 orientation[25]. There is some inconsistency in the literature regarding this assumption[25, 26], but it is also known that fabrication conditions, such as temperature, would influence preferential growth[8, 25]. Furthermore, the only condition for our interpretation is that N increases monotonically and that $\underline{\gamma}(100)$ also increases. If it was the case that $\underline{\gamma}(002) > \underline{\gamma}(100)$, as opposed to our assumption here, the condition would be that N increases slower than $\underline{\gamma}(100)$ and we do not dismiss this possibility in future studies. In any case, considering our data in Figure 2 the assumption seems reasonable. With the aid of (6) and this latter assumption we can now make qualitative predictions in terms of the expected behaviour of the mean surface energy measured by an AFM for a given SA as a function of Hf concentration or number of cycles as described in Table I. Such discussion follows.

SITUATION ONE (undoped ZnO case): We first assume that M>>N (Figure 1) and that $\underline{\gamma}(002) > \underline{\gamma}(100)$ for the undoped case (ZnO). According to Eq. (6) this results in a mean surface energy that we can write as $\underline{\gamma}(ZnO)$ for the undoped case. This gives us a baseline for our next considerations.

SITUATION TWO (low Hf concentration, HZO-L case): if we measure any increase in surface energy with the AFM relative to the baseline, that is, if $\underline{\gamma}(ZnO) < \underline{\gamma}(HZO\text{-}L)$, and assuming $\underline{\gamma}_{002}$ to be constant, the situation can be potentially explained by our hypothesis of substitution of Hf into the 100 crystals since this implies a direct increase in $\underline{\gamma}(100)$ manifested as $\underline{\gamma}(ZnO) < \underline{\gamma}(HZO\text{-}L)$. The contribution to higher surface energy on the other hand could be also due to crystal orientation alone, i.e. it could follow directly from larger N together with the $\underline{\gamma}(002) > \underline{\gamma}(100)$ assumption. It therefore follows that no Hf substitution mechanism would be necessary to explain the increase in $\underline{\gamma}$. Nevertheless, as we have discussed, the monotonic increase in N (Figure 2) cannot explain non-monotonic behaviour provided the mechanism is explained by crystal orientation alone. Thus, we discard this hypothesis. On the other hand, if Hf substitution was the main contributor to mean surface energy, as predicted by Figure 2, our hypothesis could explain non-monotonicity. We will discuss this below. Initially, the only assumption is that N is sufficiently small that enough 100 oriented crystals provide sites for substitution. More formally, independently of the initial N/M ratio, the rate of change of N is initially expected to be lower than that of $\underline{\gamma}(100)$. Provided the condition $\underline{\gamma}(002) > \underline{\gamma}(100)$ is sustained however, $\underline{\gamma}(HZO\text{-}L)$ should be necessarily lower than $\underline{\gamma}(002)$.

SITUATION THREE (middle or medium Hf concentration, HZO-M case): if we experimentally obtained that $\underline{\gamma}(ZnO\text{-}L) < \underline{\gamma}(HZO\text{-}M)$ with the AFM, the same discussion given in case two would be valid. It is even possible however that there is a point where $\underline{\gamma}_{100}$ is sufficiently large due to Hf substitution that the relative surface energy condition is now inverted. That is, we could get a situation where $\gamma(002) < \underline{\gamma}(100)$ due to high enough Hf substitution in the 100 crystal orientation sites. In such case $\gamma(HZO\text{-}M)$ would be larger than $\underline{\gamma}(002)$ according to Eq. (6). This situation could not be explained by crystal orientation and its relation to surface energy alone but could still explain monotonicity.

SITUATION FOUR (high Hf concentration, HZO-H case): we would reach the more interesting case where even by assuming that $\gamma(002) << \underline{\gamma}(100)$, that is, even by increasing Hf substitution to the point where substitution sites might saturate, N would now be so large that the contribution due to M, that is, due to the highly doped 100 crystals, would be negligible. This is a consequence of the relationship between 100 and 002 presence as shown in Figure 1. In the extreme case we could find for $N \rightarrow 1$ and $M \rightarrow 0$ that (HZO-H case):

$$\gamma(002) << \underline{\gamma}(100) \quad (7)$$

$$\underline{\gamma} \approx \underline{\gamma}_{002} \quad (8)$$

If substitution occurred only in M sites, the above conditions alone would be sufficient to explain the non-monotonic behaviour in optoelectronic properties with Hf concentration or cycles during manufacturing as described in the introduction, the methods section and in the literature. In summary, the simplicity of this interpretation makes it appealing and provides a pathway to the investigation of property manipulation via Hf doping of ZnO films.

In order to experimentally verify the actual behaviour of the mean surface energy during AFM scans we imaged the set of samples from undoped ZnO to highly doped (HZO-H). Since the surface energy ratio would provide the mechanism for contrast as explained by Eqs. (1) and (4), we opted for the simple case of transforming the AFM data into direct adhesion force F_{AD} maps. As observed by inspecting Eq. (1) the only mechanism for contrast would indeed be the surface energy. Recently, we have shown that it is possible to operate the AFM in the standard AM AFM mode and directly compute the force of adhesion per pixel while raster scanning. This is achieved

by sufficiently decreasing the set point A_{sp} relative to the free amplitude A_0[15]. In such cases the adhesion force F_{AD} is simply the product:

$$F_{AD} \approx -kz_0 \qquad (9)$$

where k is the cantilever's spring constant and z_0 is the cantilever's mean deflection. In Figure 3 we show a topography (Figure 3a) scan for a ZnO undoped film and the corresponding force of adhesion map (Figure 3b). The contrast in F_{AD} (Figure 3) can be directly interpreted as $\gamma(002) > \gamma(100)$ for the ZnO case by assuming that there are 002 sites and 100 sites and that the 002 sites give rise to the domains where F_{AD} is larger (toward green and yellow in Figure 3b) whereas the 100 sites give rise to the domains where F_{AD} is lower (toward blue in Figure 3b). In Figure 3c we provide an example of two force versus distance curves reconstructed directly from observables in the high (green curve) and low (blue curve) F_{AD} regions in Figure 3b. We note that we interpret high and low adhesion in absolute terms where high means high adhesion and low means low adhesion.

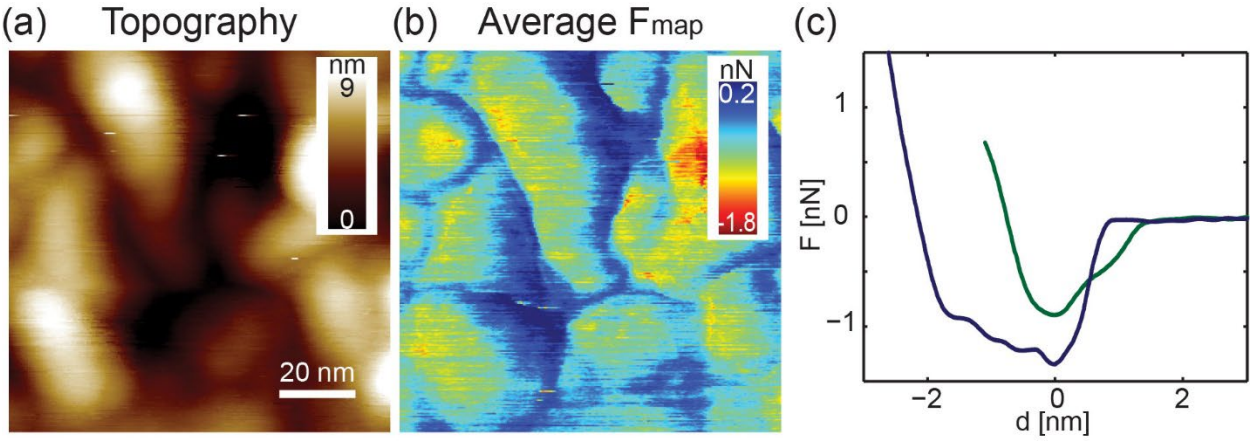

Figure 3. The topography (a) image of ZnO, the corresponding adhesion map (b), and representative reconstructed force profiles (c) taken from the spots indicated in Figure 1.

We obtained F_{AD} maps for the four cases (Table I) as described above in the four situations discussed in order to interpret Eq. (6). The results are shown in Figure 4. We acquired five consecutive 1 by 1 μm scans for each case. By looking at the size of the crystal domains in Figure 3b and noting that these are in the 100s of nm^2 per crystal, we assume that the 5,000,000 nm^2 effectively scanned in our experiments for each case provide us an area large enough to obtain robust statistics. The trends observed in the adhesion force maps is in very good agreement with our interpretation (Figure 4). First, the tendency is for the adhesion force to increase with Hf concentration up to HZO-M. Above these Hf concentrations the mean surface energy tends to decrease (Figure 4a). The mean values and standard deviations measured in our experiments are plotted in Figure 4b. This behaviour is indeed non-monotonic and might explain the optoelectronic behaviour as expected and as interpreted here – see discussion of the 4 possible situations above.

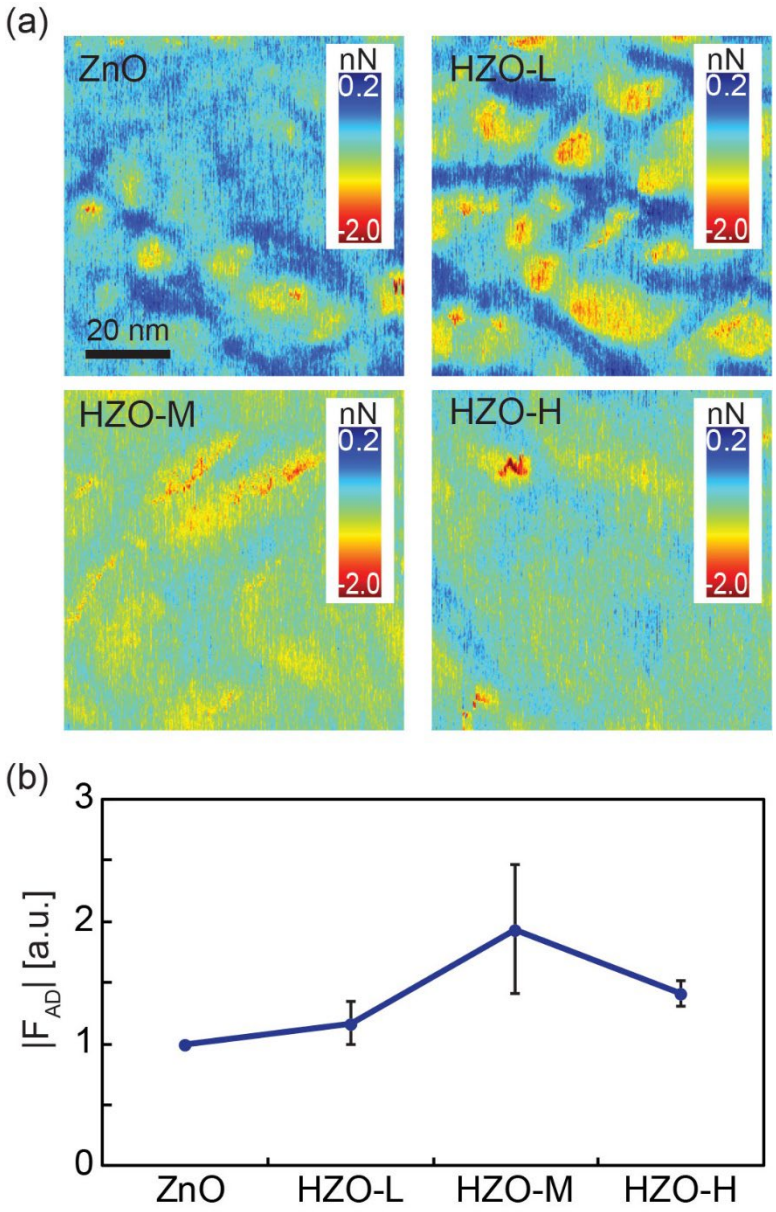

Figure 4. (a) Adhesion maps for the undoped ZnO case and the HZO (doped cases) thin films and (b) the corresponding average adhesion force.

We have recently shown that besides the adhesion force it is possible to obtain Hamaker H maps directly by exploiting multifrequency AM AFM[27]. Experimentally, we conducted 5 more scans per each case in Table I and transformed the data into H maps. The images in Figure 5 are particularly revealing in that we observe that the regions where H is highest are obtained for the

HZO-M case. This is what we would expect for a scenario where substitution occurs only, or mostly, for a single crystal orientation case as is our hypothesis. In particular, if we identify high H values with crystals with the 100 orientation, we see an inflexion point occurs for HZO-M as we discussed above. In Figures 5b and 5c we provide a histogram containing the distributions for all the data sets and a plot displaying the behaviour of the mean surface energy as transformed from the value of H. We discuss any possible pitfalls of our assumptions in the conclusion.

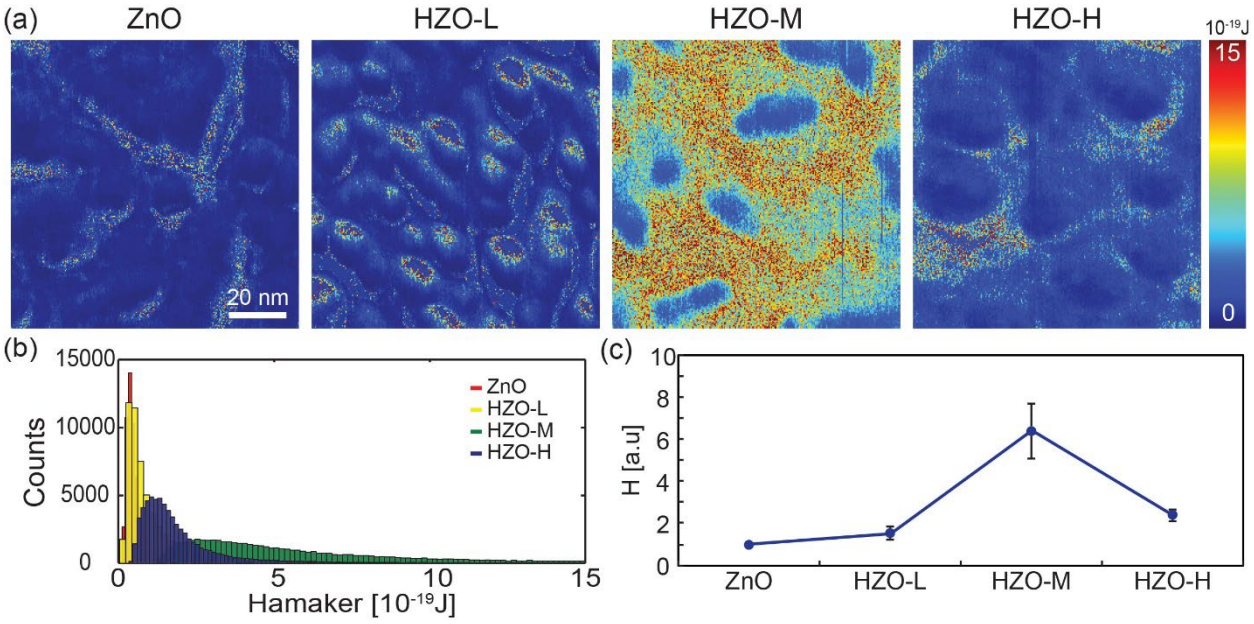

Figure 5. Hamaker coefficients mapping of ZnO and HZO films (a), distribution (b), and the change of mean Hamaker coefficients with respect to different Hf doping (c).

IV. Conclusion

We have shown that it is possible to interpret the non-monotonic behaviour in optoelectronic properties for Hf doped (ZnO based) semiconductor films by considering two competing

mechanisms. Specifically, we propose that provided two crystal orientations dominate film growth, only one of them might be responsible for direct Hf substitution. We propose that this is the ZnO 100 crystal orientation. Non-monotonic behaviour is expected at once by considering that the preferential growth of the 100 orientation occurs only in the undoped or low Hf concentration scenarios. Thus, increasing Hf concentration, or cycles, during the fabrication processes inhibits precisely the crystal that is targeted for Hf substitution. Maxima in Hf substitution is reached at a point where enough crystals exhibit the 100 orientation and enough Hf is present on the surface for substitution. Outside such optimum case, Hf substitution can only decrease. We note however that our main contribution here is not based on our choice of parameter claimed to contribute to the competing mechanism only. That is, even though we have assumed that it is only a single crystal orientation that contributes to Hf substitution, our more general hypothesis consists in 1) selecting a parameter N – here the 002 crystal orientation - that increases with Hf concentration and 2) that Hf substitution is a function of x(1-N), where x also increases with Hf concentration. In our particular hypothesis x is the surface energy associated with (1-N)=M domains. In short, our claim is that even if our 1) identification of the relevant parameter x as surface energy, 2) our association of surface energy with Hf substitution and 3) our identifying the normalised area 1-N with the crystal associated with x was refuted in future experiments or work, our more general hypothesis attempting to explain non-monotonic behaviour might still be valid by considering alternative phenomena controlling (1-N). For example, it might be shown in the future that associating N with the crystal orientation 002 does not predict experimental outcomes. This would refute only our claim that Hf substitutes only in the 100 oriented crystal. In such case our hypothesis could be modified by considering that N should be identified with a given shape or morphology of the crystals[7] rather than with crystal orientation since these also vary with Hf

concentration[8]. The conclusions would remain identical with these alternative considerations and would indicate that the mechanism competing for the net surface energy, and therefore Hf substitution, would be shape and morphology rather than orientation.

Acknowledgements

C.Y. L, C.Y. L, S. S. and M.C. acknowledge the support of the Arctic Center for Sustainable Energy (ARC), UiT Arctic University of Norway through grant no. 310059.

References

1. N. W. Ashcroft and D. N. Mermin, *Solid State Physics*, Cengage Learning1976.
2. E. Fortunato, P. Barquinha and R. Martins, *Advanced Materials*, 2012, **24**, 2945-2986.
3. N. S. Rajput, Y. Shao-Horn, X.-H. Li, S.-G. Kim and M. Jouiad, *Physical Chemistry Chemical Physics*, 2017, **19**, 16989-16999.
4. Y. Lin, W.-J. Chen, J. Y. Lu, Y. H. Chang, C.-T. Liang, Y. F. Chen and J.-Y. Lu, *Nanoscale research letters*, 2012, **7**, 401.
5. H. Y. Chao, S. H. You, J. Y. Lu, J. H. Cheng, Y. H. Chang, C. T. Liang and C. T. Wu, *Journal of Nanoscience and Nanotechnology*, 2011, **11**, 2042-2046.
6. C.-F. Chien and R.-T. Kuo, *Flexible Services and Manufacturing Journal*, 2013, **25**, 310-342.
7. S. C. Erwin, L. Zu, M. I. Haftel, A. L. Efros, T. A. Kennedy and D. J. Norris, *Nature*, 2005, **436**, 91-94.
8. B. Alfakes, J. Villegas, H. Apostoleris, R. Devarapalli, S. Tamalampudi, J.-Y. Lu, J. Viegas, I. Almansouri and M. Chiesa, *The Journal of Physical Chemistry C*, 2019, **123**, 15258-15266.
9. I. Staude and J. Schilling, *Nature Photonics*, 2017, **11**, 274.
10. L. C. Feldman, *Fundamental Aspects of Silicon Oxidation*, Springer2012.
11. A. G. Aberle, *Progress in Photovoltaics: Research and Applications*, 2000, **8**, 473-487.
12. B. Alfakes, C. Garlisi, J. Villegas, A. Al-Hagri, S. Tamalampudi, N. S. Rajput, J.-Y. Lu, E. Lewin, J. Sá, I. Almansouri, G. Palmisano and M. Chiesa, *Surf. Coat. Technol.*, 2020, **385**, 125352.
13. N. S. Rajput, S.-G. Kim, J. B. Chou, J. Abed, J. Viegas and M. Jouiad, *MRS Advances*, 2016, **1**, 825-830.
14. C.-Y. Lai, T. Olukan, S. Santos, A. Al Ghaferi and M. Chiesa, *Chem. Commun.*, 2015, **51**, 17619-17622.
15. S. Santos, *Applied physics letters*, 2013, **103**, 231603.
16. S. Santos, L. Guang, T. Souier, K. R. Gadelrab, M. Chiesa and N. H. Thomson, *Review of Scientific Instruments*, 2012, **83**, 043707-043717.
17. J. Israelachvili, *Intermolecular & Surface Forces*, Academic Press, New York, 1991.

18. R. Garcia and A. San Paulo, *Physical Review B*, 1999, **60**, 4961.
19. C.-Y. Lai, S. Perri, S. Santos, R. Garcia and M. Chiesa, *Nanoscale*, 2016.
20. R. García and R. Pérez, *Surface Science Reports*, 2002, **47**, 197-301.
21. Y. Geng, Z.-Y. Xie, W. Yang, S.-S. Xu, Q.-Q. Sun, S.-J. Ding, H.-L. Lu and D. W. Zhang, *Surface and Coatings Technology*, 2013, **232**, 41-45.
22. H. Ibach, *Physics of surfaces and interfaces*, Springer2006.
23. V. K. Tewary, *Journal of Physics F: Metal Physics*, 1973, **3**, 704-708.
24. H. Morkoç and Ü. Özgür, *Zinc Oxide: Fundamentals, Materials and Device Technology*, Wiley-VCH2009.
25. N. Fujimura, T. Nishihara, S. Goto, J. Xu and T. Ito, *Journal of Crystal Growth*, 1993, **130**, 269-279.
26. A. U. Pawar, C. W. Kim, M. J. Kang and Y. S. Kang, *Nano Energy*, 2016, **20**, 156-167.
27. C.-Y. Lai, S. Perri, S. Santos, R. Garcia and M. Chiesa, *Nanoscale*, 2016, **8**, 9688-9694.
28. P. Giannozzi, O. Andreussi, T. Brumme, O. Bunau, M. Buongiorno Nardelli, M. Calandra, R. Car, C. Cavazzoni, D. Ceresoli, M. Cococcioni, N. Colonna, I. Carnimeo, A. Dal Corso, S. de Gironcoli, P. Delugas, R. A. DiStasio, A. Ferretti, A. Floris, G. Fratesi, G. Fugallo, R. Gebauer, U. Gerstmann, F. Giustino, T. Gorni, J. Jia, M. Kawamura, H. Y. Ko, A. Kokalj, E. Küçükbenli, M. Lazzeri, M. Marsili, N. Marzari, F. Mauri, N. L. Nguyen, H. V. Nguyen, A. Otero-de-la-Roza, L. Paulatto, S. Poncé, D. Rocca, R. Sabatini, B. Santra, M. Schlipf, A. P. Seitsonen, A. Smogunov, I. Timrov, T. Thonhauser, P. Umari, N. Vast, X. Wu and S. Baroni, *J. Phys.: Condens. Matter*, 2017, **29**, 465901.